Journal of Power Sources 220 (2012) 264–268

Contents lists available at SciVerse ScienceDirect

Journal of Power Sources

journal homepage: www.elsevier.com/locate/jpowsour

Short communication

# Enhanced electrochemical performance of $LiFePO_4$ cathode with in-situ chemical vapor deposition synthesized carbon nanotubes as conductor

Xiaoran Sun, Jiajun Li, Chunsheng Shi, Zhiyuan Wang, Enzuo Liu, Chunnian He, Xiwen Du, Naiqin Zhao*

*School of Materials Science and Engineering, and Tianjin Key Laboratory of Composite and Functional Materials, Tianjin University, Weijin Road 92#, Tianjin 300072, China*

## HIGHLIGHTS

- ► CNTs/$LiFePO_4$ composite was prepared by in-situ chemical vapor deposition method.
- ► It shows superior electrochemical performance over the mechanical mixture.
- ► The interface bonding between $LiFePO_4$ and in-situ synthesized CNTs are excellent.

## ARTICLE INFO

*Article history:*
Received 8 June 2012
Received in revised form
20 July 2012
Accepted 28 July 2012
Available online 11 August 2012

*Keywords:*
Lithium iron phosphate
Carbon nanotubes
In-situ synthesis
Lithium-ion battery
Fast charge/discharge

## ABSTRACT

In this paper, carbon nanotubes (CNTs) are added in order to investigate their influence on the electronic conductivity of $LiFePO_4$ cathode. CNTs/$LiFePO_4$ composites are prepared by in-situ chemical vapor deposition method and the traditional mechanical mixture method respectively in order to investigate the influence of CNTs as an additive on the electrochemical performance of $LiFePO_4$ cathode. The particle morphology and electrochemical performances of the CNTs/$LiFePO_4$ composites are characterized and compared with commercial cathodes, $LiFePO_4$ mixed with carbon black. The in-situ synthesized CNTs/$LiFePO_4$ composite by chemical vapor deposition method maintains full retaining ratio after 100 cycles at 1C and 94.5% retention after 20 cycles at 10C, which precede the CNTs/$LiFePO_4$ composite fabricated by the mechanical mixture method as well as the commercial cathode. The enhanced electrochemical performance is due to the excellent interface bonding between $LiFePO_4$ and CNT in in-situ synthesized CNTs/$LiFePO_4$ composites. The interface benefits the electronic conductivity of the composites, as well as the polarization reduction.



## 1. Introduction

Lithium iron phosphate ($LiFePO_4$, LFP), once discovered [1], has been considered as one of the most promising cathode materials for lithium-ion battery. The main advantages of $LiFePO_4$ are flat voltage profile, good electrochemical/thermal stability, relatively low cost for synthesis, and environmental compatibility with less toxic than $LiCoO_2$ and $Li_2MnO_3$ [2,3]. However, its low electronic conductivity and lithium-ion diffusivity across the $LiFePO_4/FePO_4$ interface restrict its electrochemical kinetics during the charge/discharge process, especially in high current density situations. Extensive efforts have been performed to improve its electrochemical performance over decades, which can be classified into the following categories: particle size/shape optimizing [4–9] and porousness morphology [10,11], different cations/anions doping [12–14], as well as coating or admixing $LiFePO_4$ particles with better conductive agents [15–17].

Among these methods used for improving electrochemical properties of $LiFePO_4$, carbon coating is one of the most frequent techniques to enhance the specific capacity, rate performance, and cycling life [18,19]. Carbon nanotubes (CNTs) and carbon nanofibers (CNFs), as advanced one-dimensional carbon materials, are used as the additives with the properties of large surface area, short diffusion path for electron transport, and high electronic/thermal conductions [20–22]. In recent years, the production process of CNTs (CNFs)/$LiFePO_4$ composite materials ranges from solid-state reaction [23,24], hydrothermal route [25] to sol–gel synthesis [11,26]. CNFs/$LiFePO_4$ composite cathodes have also been synthesized via microwave pyrolysis chemical vapor deposition (CVD) method and CVD method combined with solid-state reaction [27,28]. In-situ CVD synthesis is a facile way to product CNTs/CNFs. It has the advantage of forming better interface between the CNTs/CNFs and the substrate over the other methods. On the other hand,

* Corresponding author. Tel./fax: +86 22 27891371.
*E-mail address:* nqzhao@tju.edu.cn (N. Zhao).

0378-7753/$ – see front matter © 2012 Elsevier B.V. All rights reserved.
http://dx.doi.org/10.1016/j.jpowsour.2012.07.082

CNTs have better conductivity than CNFs, so that they are more likely to promote the electrochemical performance of $LiFePO_4$ cathode theoretically.

In the present work, CNTs/$LiFePO_4$ composite powders were synthesized by in-situ CVD method first time. The CNTs/$LiFePO_4$ composite powders by the traditional mechanical mixture method are also prepared as the comparative sample. Their conductivity was measured via four-probe method and electrochemical impedance spectra (EIS). The electrochemical performances of the CNTs/$LiFePO_4$ electrodes were tested and compared with the performances of the cathode generally used in the commercial batteries. Based on the morphology observation of each sample, the interface effect on the electrochemical properties of $LiFePO_4$ was analyzed. The results are helpful in fabricating CNTs/$LiFePO_4$ materials with high-rate capability for lithium-ion batteries.

## 2. Experimental

### 2.1. Preparation of CNTs/$LiFePO_4$ composites

*CNTs/$LiFePO_4$ Synthesized by in-situ chemical vapor deposition method*. Firstly, adequate amounts of $Co(NO_3)_2 \cdot 6H_2O$ (99% purity) as the catalyst precursor and lithium iron phosphate powder (Aleees, $D_{50} = 1.921$ μm) as the carrier were mixed in distilled water in the mass ratio of 1:200 (Co: $LiFePO_4$). Then sufficient NaOH (96% purity) was dissolved in distilled water and added slowly to the previous mixture with constant stirring for the precipitation of $Co(OH)_2$. To form the catalyst precursor supported on $LiFePO_4$ particles, the binary colloid ($Co(OH)_2$/$LiFePO_4$) obtained was washed, dried, ground, and calcined in an Ar atmosphere at 200 and 400 °C continuously for 2 h each. The obtained precursor powder was placed in a quartz boat in the middle of a tube furnace and reduced at 450 °C under a flow of 100 sccm of $H_2$ for 1 h, followed by the CNTs growth at 675 °C in a gas mixture of 7 sccm of $C_2H_2$ and 350 sccm of Ar for 30 min. Lastly, the sample (marked as CNTs/LFP-1) was slowly cooled to room temperature under Ar protection.

*CNTs/$LiFePO_4$ prepared using the mechanical mixture method.* Dispersant (Hexadecyldimethyl (3-sulfopropyl) ammonium Hydroxide Inner Salt, TCI) was dissolved in distilled water at 50 °C, followed by slowly adding CNTs (Chengdu Organic Chemicals Co. Ltd., >95% purity) and $LiFePO_4$ powder into it. The mixture was then dispersed ultrasonically for 30 min. After filtration, drying, and calcination at 500 °C in Ar atmosphere for 1 h to remove the dispersant, the composite powder (marked as CNTs/LFP-2) was obtained.

In order to make clear the effect of CNTs on the electrochemical performances of $LiFePO_4$ electrode, the comparative sample, which is generally used in the commercial batteries, was made by mixing raw materials and conductive acetylene black (carbon black, CB) in the weight ratio of 80:10 (marked as CB/LFP). It has the same carbon content with CNTs/LFP-1 and CNTs/LFP-2 through carbon and sulfur analyzer testing (approximately 13%).

### 2.2. Characterization

The microstructure and morphology of the composite powder were investigated by field emission scanning electron microscope (FESEM, HITACHI S4800) and high-resolution transmission electron microscope (HRTEM, PHILIPS TECNAI $G^2$ F20). The phase identification of products was carried out using X-ray diffraction (XRD, Rigaku D/max-2500, Cu–Kα radiation) in the 2θ range from 15° to 80°. In addition, the carbon content of products was measured by high frequency infrared carbon and sulfur analyzer (Beijingwld, CS-910B).

### 2.3. Electrochemical measurements

The coating slurry comprises as-obtained composite powder and polyvinylidene fluoride (PVDF) binder, which were mixed in N-methylpyrrolidone (NMP) in the weight ratio of 90:10. After 3–4 h of stirring, the slurry was spread on Al foil current collector and dried under vacuum at 110 °C overnight. The CR2032-type coin cells were assembled in an Ar-filled glovebox using metallic lithium as anode, 1 M $LiPF_6$ solution in ethylene carbonate (EC)/ethyl methyl carbonate (EMC)/dimethyl carbonate (DEC) (1:1:1 in volume) as electrolyte, and Celgard 2300 porous polypropylene film as diaphragm.

The cells were galvanostatically charged and discharged under different current densities between 2.0 V and 4.3 V (vs. $Li/Li^+$) using a CT2001A cell test instrument (LAND Electronic Co.) where 1C corresponds to 170 mA $g^{-1}$. Cyclic Voltammograms (CV) were conducted between 2.5 V and 4.3 V at 0.1 mV $s^{-1}$ using a CHI660D electrochemical workstation. Electrochemical Impedance Spectroscopy (EIS) measurements were made using electrochemical workstation (PARSTAT2273, Priceton) in the frequency range of 100 kHz to 0.01 Hz. The electronic conductivity of the samples was measured by using the four-point probe method. All tests were carried out at room temperature.

## 3. Results and discussion

The first charge/discharge curves of the CB/LFP and CNTs/LFP samples at the current rate of 0.1C are shown in Fig. 1. As there is no capacity in carbon, all samples exhibit capacities less than theoretical value. The discharge capacities of Sample CB/LFP and CNTs/LFP-1 reach up to 161.2 and 160.1 mAh $g^{-1}$ respectively. For Sample CNTs/LFP-2, the value is only 155 mAh $g^{-1}$. The flat plateaus can be observed both in charge curves (3.46 V) and discharge curves (3.40 V), which indicate the good crystallization of $LiFePO_4$, in agreement with the X-ray diffraction spectrum (Fig. 2). Although their preliminary treatments are different, all samples present very similar XRD spectrums to that of the major phase of orthorhombic $LiFePO_4$ (JCPDS: 40-1499). No signs of crystalline $Fe_2P$, $Li_3PO_4$ or other impurities are observed in the X-ray pattern. This manifests the pureness of as-obtained samples.

The charge (Li extraction) and discharge (Li reinsertion) curves at various rates are presented in Fig. 3. In these electrochemical tests, all samples were charged at 0.1C, and discharged at current

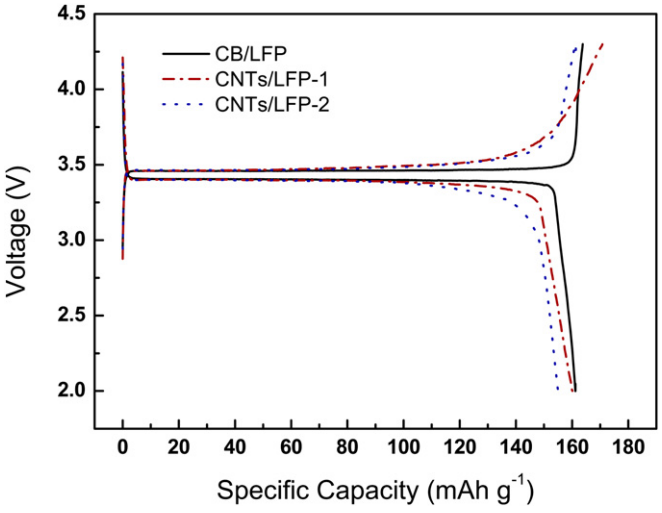


**Fig. 1.** First charge–discharge profiles of carbon/$LiFePO_4$ composite samples.

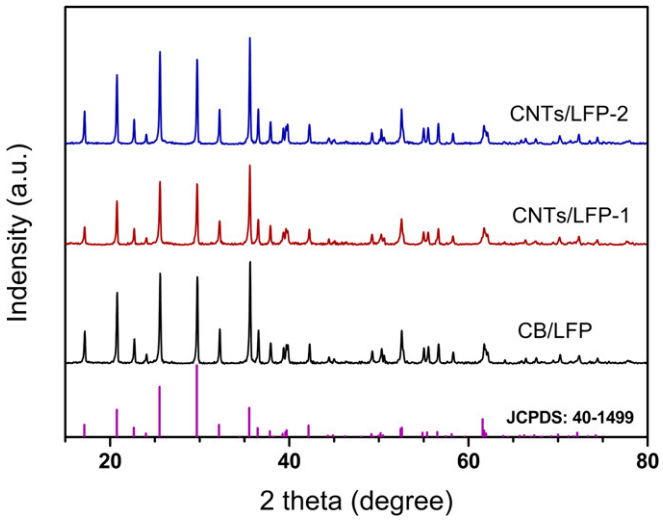


**Fig. 2.** XRD patterns of carbon/$LiFePO_4$ composite samples.

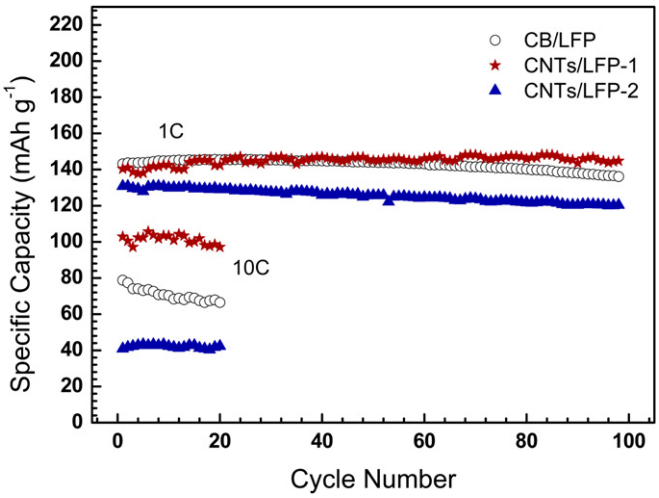


**Fig. 4.** The cyclic performance of carbon/$LiFePO_4$ composites.

rates of 0.1C, 1C, 2C, 5C, and 10C. At relatively low current rates (0.1C, 1C, 2C, 5C), the Sample CNTs/LFP-1 maintains almost the same capacity with the Sample CB/LFP, while the capacity of Sample CNTs/LFP-2 decreases intensively. It is noteworthy that the Sample CNTs/LFP-1 also gives the highest capacity at high current density. During 10C rate, a discharge capacity of 101 mAh $g^{-1}$ can be obtained for the Sample CNTs/LFP-1, while for Sample CB/LFP and CNTs/LFP-2, the values rapidly drop to 84 and 43 mAh $g^{-1}$. The high-capacity at large rate illustrates a faster electronic conductivity and lithium-ion diffusivity in Sample CNTs/LFP-1. The cyclic performance of carbon/$LiFePO_4$ cathodes are shown in Fig. 4. The capacities of the three samples are 136.1, 144.8, and 120.4 mAh $g^{-1}$, respectively, and the retaining ratios are 95%, 100%, and 92% after 100 circles. The cycle data at 1C strongly indicates an excellent cycling stability for the Sample CNTs/LFP-1. Moreover, unmatched reversibility of this composite cathode is also demonstrated at higher current density. The Sample CNTs/LFP-1 exhibits an excellent capacity (97.2 mAh $g^{-1}$, 94.5% retention) after 20 cycles at 10C over the other two samples.

On the other hand, the polarization presented in current–voltage profiles suggests the electrochemical kinetics. The fifth circles of three samples are shown in Fig. 5. In each cycle, the main anodic peak and cathodic peak can be found, corresponding to the two-phase charge/discharge reaction of the $Fe^{2+}/Fe^{3+}$ redox couple. The Sample CNTs/LFP-2 is advantageous to the cathode performance due to a smaller voltage interval between its anodic and cathodic peaks than that between the Sample CB/LFP's. However, the fatal drawback of the reversibility restricts its development. Among these three samples, CNTs/LFP-1 has the smallest potential difference between symmetrical redox peaks (0.220 V) and the highest peak currents, indicating it has the smallest electrode polarization and the best electrode kinetics. Moreover, the redox reaction is more quickly and completely in Sample CNTs/LFP-1 due to its better conductivity. Consequently, there is much more proportion of active material reacting in the Sample CNT/LFP-1 compared to the Sample CB/LFP under the same potential sweep rate, which causes the phenomenon that the area of CV peaks measured with Sample CNTs/LFP-1 is much smaller than that measured with Sample CB/LFP.

It is known that the electronic conductivity is one of the key factors to affect the electrochemical performances of the electrode. The electrochemical performance improvements (including high-rate capacity enhancement, cycle performance promotion and electrode polarization decrease) of the in-situ CVD sample could be greatly attributed to the high electronic conductivity of the sample.

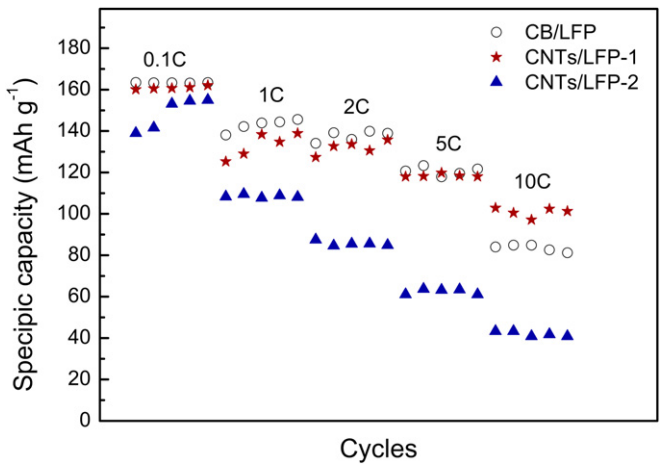


**Fig. 3.** The rate capacity of carbon/$LiFePO_4$ composites.

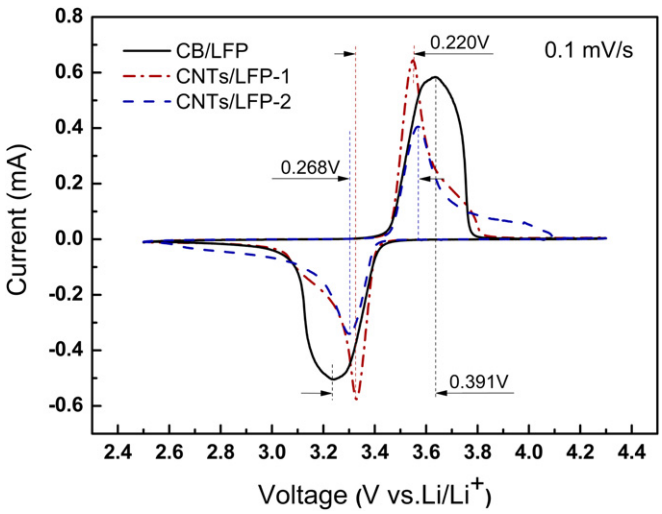


**Fig. 5.** Cyclic voltammograms recorded for the carbon/$LiFePO_4$ composites.

**Table 1**
Electronic conductivity (S $cm^{-1}$) of different samples.

| Raw material | CB/LFP | CNTs/LFP-1 | CNTs/LFP-2 |
|---|---|---|---|
| $1.75 \times 10^{-3}$ | 0.284 | 0.615 | 0.188 |

**Table 2**
The impedance parameters of equipment circuits.

| Sample | $R_s$ ($\Omega$ $cm^{-2}$) | $R_{SEI}$ ($\Omega$ $cm^{-2}$) | $R_e$ ($\Omega$ $cm^{-2}$) | $R_{ct}$ ($\Omega$ $cm^{-2}$) | $W$ (S $sec^{0.5}$ $cm^{-2}$) |
|---|---|---|---|---|---|
| CB/LFP | 2.875 | 75.34 | 131.5 | 54.97 | 0.02374 |
| CNTs/LFP-1 | 2.665 | 107.5 | 100.6 | 17.51 | 0.01834 |
| CNTs/LFP-2 | 2.521 | 129.7 | 120.4 | 23.62 | 0.008263 |

Therefore, the electronic conductivity of the samples is investigated in the following.

The electronic conductivity values of different samples are listed in Table 1. The electronic conductivity of the three as-obtained samples is several orders of magnitude larger than that of raw $LiFePO_4$. Sample CNTs/LFP-1 has the highest conductivity. This advantage of the in-situ synthesized sample over the mechanically mixed one may result from a more homogeneous contact between CNTs and LFP of the composite formed during the process of in-situ CVD growth.

EIS measurements were performed under the open-circuit voltage of each cell and the potentiostatic signal amplitude of 20 mV. The cells were activated five cycles at 0.1C before testing. The parameters of equipment circuit in impedance spectra were simulated by ZSimpWin 3.00 and the results are listed in Table 2. According to the schematic diagram of the composite material (Fig. 6(a)), the impedance spectra of all samples are combinations of depressed semicircles in high frequency region and straight lines in low frequency region, as shown in Fig. 6(b). The intercept at $x$ axis corresponds to the ohmic resistance ($R_s$), which includes the electrolyte resistance, particle contact resistance and other physical resistances. The depressed semicircle in high frequency relates to the Li-ion migration resistance ($R_{SEI}$) through SEI film formed on cathode surface. The following depressed semicircles indicate the electron transport resistance ($R_e$) [29], then the charge transfer resistance ($R_{ct}$) in intermediate frequency area. The oblique line in low frequency area denotes the Warburg impedance ($W$), which is

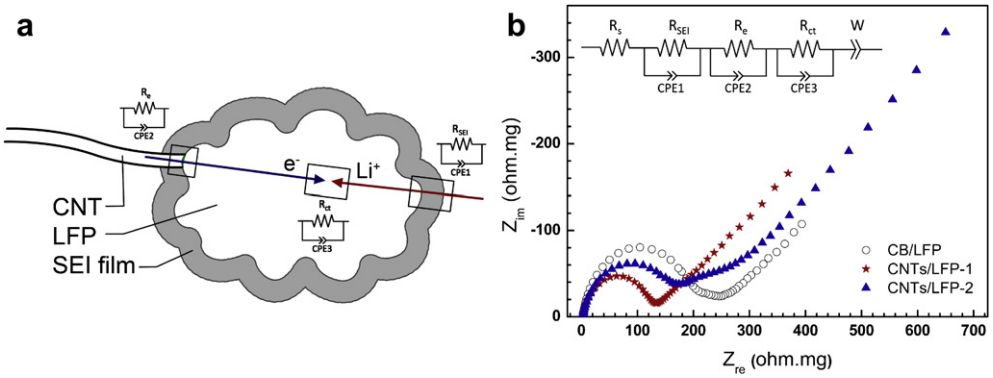


**Fig. 6.** (a) Schematic diagram of the CNTs/LFP-1 composite material; (b) the AC impedance spectra of carbon/$LiFePO_4$ composites.

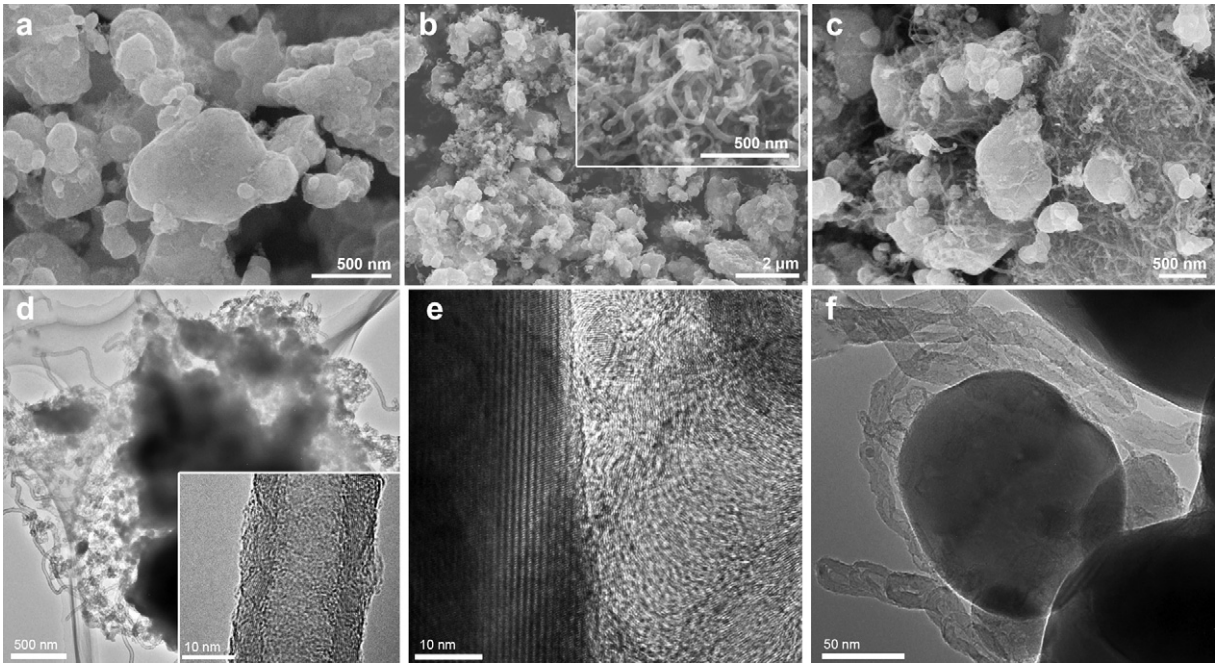


**Fig. 7.** SEM and HRTEM pictures of raw $LiFePO_4$ powder (a), CNTs/LFP-1(b, d, and e), and CNTs/LFP-2 (c and f). Inset in (b) and (d) show the magnifying image of the growing fishbone-like CNTs.

associated with lithium-ion diffusion in active material. Since the major difference in electron transport resistance among samples is the carbon/$LiFePO_4$ interface resistance, the noticeable decrease of $R_e$ illustrates in-situ synthesis of CNTs is an effective method to reduce the interface resistance. At the same time, the decrease of interface resistance leads to a rise of electron concentration at the interface per unit time. Because of the increase of electron concentration, the electron transfer speed in $LiFePO_4$ gets faster, and hence $FePO_4$/$LiFePO_4$ phase reaction becomes more quickly. This could result in the diminution of $R_{ct}$. In general, the decrease of $R_e$ and $R_{ct}$ demonstrates the electronic conductivity has been improved in working cathode, which is in agreement with the tendency discovered in the study of powder conductivity.

In order to investigate the mechanism of electronic conductivity promotion, the morphologies and structures of the samples were observed by the scanning electron microscopy and the transmission electron microscopy. SEM images show that the original powder consists of micro-sized secondary particles with agglomeration (Fig. 7(a)). CNTs can be observed on the surface of $LiFePO_4$ powders after the CVD (Fig. 7(b)) and mechanical mixture process (Fig. 7(c)). The CNTs obtained via CVD are dispersed on the substrate uniformly, whose length range from tens to hundreds of nanometers. TEM images taken reveal more details of the nanoproducts. The obtained CNTs are multi-walled CNTs composed of about 20 graphite layers and have a tubular structure with the average diameter of 25 nm, as shown in Fig. 7(d). The interlayer space of CNTs is about 0.3438 nm, corresponding to the lattice distance between the (002) planes of graphite. Fig. 7(e) and (f) illustrate a better interface between CNTs and $LiFePO_4$ substrate in the CNTs/LFP-1 sample than that in the mechanical mixture.

It has been widely confirmed that all parts of the $Li^+$-electron path have to be capable of sustaining capacity, and electron transport is a more influential determining factor than Li-ion delivery. CNTs additive provides less value to $R_e$ and $R_{ct}$ than carbon black does because CNTs facilitate the electron transport, thus being considered as a better conductive additive [30]. Compared with traditional mechanical mixing, CNTs synthesized by in-situ CVD is able to build a homodispersed three-dimensional network, which is beneficial to reducing the electrode polarization of batteries and constructing a better interface as well. The compact integration at the interface will open the way for building atom connections, then chemical bonding between surface C atoms and O atoms from $PO_4$ tetrahedral units as previous reported [31]. Therefore, we speculate that the in-situ CVD synthesis promotes the charge transfer across the interface by establishing a tighter and more uniform connection, leading to the reduction of the charge transfer resistance and the increase of the electronic conductivity. Owing to the increased electronic conductivity and the improved electrochemical performance, the in-situ synthesis of CNTs/$LiFePO_4$ composite will help bring a bright future to fast-charge Li-ion battery cathode materials.

## 4. Conclusion

CNTs/$LiFePO_4$ composite cathodes were produced using in-situ chemical vapor deposition method and the traditional mechanical mixture method. The improvements of the electrochemical performance of $LiFePO_4$ cathodes, including high-rate capacity, cycle stability and electrode polarization, are obtained by the in-situ CVD synthesis. The enhanced electrochemical performance is due to the superior electronic conductivity which results from the excellent interface binding in in-situ synthesized CNTs/$LiFePO_4$ composites. Further achievement of the in-situ CVD synthesis can be expected in fast-charge lithium-ion batteries.

## Acknowledgment

This work was supported by the National Natural Science Foundation of China (Grants No. 51071107), the National Basic Research Program of China (Grants No. 2010CB934700), and the Innovation Foundation of Tianjin University.

## References

[1] A.K. Padhi, K.S. Nanjundaswamy, J.B. Goodenough, J. Electrochem. Soc. 144 (1997) 1188–1194.
[2] W.-J. Zhang, J. Power Sources 196 (2011) 2962–2970.
[3] S.L. Shang, Y. Wang, Z.G. Mei, X.D. Hui, Z.K. Liu, J. Mater. Chem. 22 (2012) 1142–1149.
[4] A. Yamada, S.C. Chung, K. Hinokuma, J. Electrochem. Soc. 148 (2001) A224–A229.
[5] D. Kim, J. Lim, V. Mathew, B. Koo, Y. Paik, D. Ahn, S.-M. Paek, J. Kim, J. Mater. Chem. 22 (2012) 2624–2631.
[6] Y. Wu, Z. Wen, J. Li, Adv. Mater. 23 (2011) 1126–1129.
[7] O. Waser, R. Büchel, A. Hintennach, P. Novák, S.E. Pratsinis, J. Aerosol Sci. 42 (2011) 657–667.
[8] M. Cuisinier, J.-F. Martin, N. Dupré, R. Kanno, D. Guyomard, J. Mater. Chem. 21 (2011) 18575–18583.
[9] S.W. Kim, J. Ryu, C.B. Park, K. Kang, Chem. Commun. 46 (2010) 7409–7411.
[10] X. Qin, X. Wang, J. Xie, L. Wen, J. Mater. Chem. 21 (2011) 12444–12448.
[11] Y. Zhou, J. Wang, Y. Hu, R. O'Hayre, Z. Shao, Chem. Commun. (Camb) 46 (2010) 7151–7153.
[12] H. Wang, Y. Yang, Y. Liang, L.F. Cui, H.S. Casalongue, Y. Li, G. Hong, Y. Cui, H. Dai, Angew. Chem. Int. Ed. Engl. 50 (2011) 7364–7368.
[13] K.-W. Nam, X.-J. Wang, W.-S. Yoon, H. Li, X. Huang, O. Haas, J. Bai, X.-Q. Yang, Electrochem. Commun. 11 (2009) 913–916.
[14] S. Adams, R.P. Rao, Physica Status Solidi (a) 208 (2011) 1746–1753.
[15] I. Lahiri, S.-W. Oh, J.Y. Hwang, S. Cho, Y.-K. Sun, R. Banerjee, W. Choi, ACS Nano 4 (2010) 3440–3446.
[16] Y. Qu, J. Cao, R. Guo, W. Xu, Electrochem. Solid-State Lett. 15 (2012) A15–A18.
[17] Y. Yin, M. Gao, H. Pan, L. Shen, X. Ye, Y. Liu, P.S. Fedkiw, X. Zhang, J. Power Sources 199 (2012) 256–262.
[18] H. Li, H. Zhou, Chem. Commun. (Camb) 48 (2012) 1201–1217.
[19] M.L. Trudeau, D. Laul, R. Veillette, A.M. Serventi, A. Mauger, C.M. Julien, K. Zaghib, J. Power Sources 196 (2011) 7383–7394.
[20] X.-M. Liu, Z.d. Huang, S.w. Oh, B. Zhang, P.-C. Ma, M.M.F. Yuen, J.-K. Kim, Compos. Sci. Technol. 72 (2012) 121–144.
[21] P.G. Bruce, B. Scrosati, J.M. Tarascon, Angew. Chem. Int. Ed. Engl. 47 (2008) 2930–2946.
[22] B. Jin, H.-B. Gu, W. Zhang, K.-H. Park, G. Sun, J. Solid State Electrochem. 12 (2008) 1549–1554.
[23] Y. Feng, Mater. Chem. Phys. 121 (2010) 302–307.
[24] L. Wang, Y. Huang, R. Jiang, D. Jia, J. Electrochem. Soc. 154 (2007) A1015–A1019.
[25] J. Xu, G. Chen, X. Li, Mater. Chem. Phys. 118 (2009) 9–11.
[26] O. Toprakci, H.A.K. Toprakci, L.W. Ji, G.J. Xu, Z. Lin, X.W. Zhang, ACS Appl. Mater. Interfaces 4 (2012) 1273–1280.
[27] C.Y. Wu, G.S. Cao, H.M. Yu, J. Xie, X.B. Zhao, J. Phys. Chem. C (2011) 23090–23095.
[28] F. Deng, X. Zeng, J. Zou, J. Huang, H. Sheng, X. Xiong, H. Qian, X. Li, Chin. Sci. Bull. 56 (2011) 1832–1835.
[29] Q.C. Zhuang, S.D. Xu, X.Y. Qiu, Y.L. Cui, L.A. Fang, S.G. Sun, Prog. Chem. 22 (2010) 1044–1057.
[30] Y. Liu, X. Li, H. Guo, Z. Wang, W. Peng, Y. Yang, R. Liang, J. Power Sources 184 (2008) 522–526.
[31] F. Pan, W.-l. Wang, D. Chen, W. Yan, J. Mater. Chem. 21 (2011) 14680–14684.